Hindawi
International Journal of Photoenergy
Volume 2020, Article ID 3013691, 11 pages
https://doi.org/10.1155/2020/3013691

Research Article

Study on the Improved Electrical and Thermal Performance of the PV/T Façade System

Ruobing Liang, Yan Gao, Peng Wang, and Chao Zhou

Faculty of Infrastructure Engineering, Dalian University of Technology, Dalian City, China

Correspondence should be addressed to Peng Wang; 31809112@qq.com

Received 21 January 2020; Accepted 11 July 2020; Published 12 August 2020

Academic Editor: Manuel Fuentes Conde

This paper is aimed at improving the performance of a building-integrated photovoltaic thermal (BIPV/T) system driven by a refrigerant pump. The research is aimed at optimizing and upgrading the BIPV/T system to address the shortcomings of the original system by replacing roll-bond PV/T units with improved heat transfer features. The system's connecting form was redesigned using a liquid separator to solve the uneven distribution of the refrigerant on the PV/T façade. We proposed the variable frequency refrigerant pump that can be adjusted to suit the working condition. An experimental study was performed to analyze the electrical and thermal efficiency of the proposed system. The results show that the electrical efficiency of the BIPV/T system was 8% which is 14.3% higher than the traditional BIPV system, while in the test period, the BIPV/T system average COP was 3.4. The thermal and comprehensive efficiencies were 20% and 42%, respectively. Besides, the proposed system's average COP was 3.7 times greater than the original BIPV/T system.

1. Introduction

Renewable energy, especially solar energy, has greatly increased, and the cost of the photovoltaic module continues to decrease as the manufacturing technology of the photovoltaic module is improved [1]. Improving electrical efficiency and thermal efficiency has become the key to solar energy utilization. However, in the process of photoelectric conversion, only a small part of the solar radiation absorbed by the solar cells is converted into electric energy, and most of the solar radiation is converted into heat energy that reduces the PV efficiency by increasing solar cell temperature [2]. The temperature of the photovoltaic module can be absorbed by appropriate natural convection or forced convection to cool the PV [3]. Consequently, various solar-assisted energy types of the system were proposed to improve the system efficiency, such as the solar-assisted heat pump system [4–7], the building-integrated photovoltaic/thermal façade system [8, 9] (BIPV/T), and the opaque ventilated solar façade integrated with PV [10].

The solar-assisted heat pump system refers to the operation of the PV/T module as an evaporator that generates electricity and produces thermal energy for heating purposes. Zhang et al. [11] studied the effect of refrigerant charge and structure parameters on the thermal performance of the system such as the optimum refrigerant charge with1.65-1.75 kg, having a solar collector area of 6.0 m^2 with 9 mm internal pipe diameter of the condenser. Lertsatitthanakorn et al. [12] used R134a as the coolant media; the COP of the solar-assisted heat pump system was 5.48. Ammar et al. [13] studied the photoelectric and photothermal conversion performance of the PV/T heat pump system with a refrigerant (R134a) as a working fluid, and the average values of COP were 6.14. Regarding the use of the roll-bond panel as the evaporator/collector, Sun et al. [14] studied the roll-bond panel with different channel patterns and concluded that the most efficient choice was the honeycomb-shaped channel pattern. Zhou et al. [15] proposed a new roll-bond PV/T unit, and the experimental result showed that the new type unit system has a large potential for building energy conservation.

The opaque ventilated solar façade is the combination of a BIPV system and the opaque ventilated façade system. The natural ventilation system reduces the temperature of the PV

cells. Ji et al. [16] studied the PV wall with and without ventilation on different orientations of the building. The results showed that the west PV wall has the greatest potential, although the ventilation PV wall has a little improvement in the electrical efficiency but can reduce much more heat gain as compared to the nonventilation system. Agathokleous et al. [17–19] analyzed a natural ventilated BIPV/T and BIPV system; the air gap between the façade and the building wall helps to reduce the heat gain of the PV panel. They also found that the modules worked stably when the air velocity is greater than 1 m/s.

The PVT heat pump system uses a refrigerant as the cooling fluid to take off the heat from the PV module. The PV/T unit acts as the evaporator of the heat pump system, the numerical [20] and experimental methods [21, 22] were conducted to analyze the performance of the system, and the conclusions showed that the average COP achieved was 6.5. The thermal and electrical efficiencies have reached 50% and 12%, respectively. Zhao et al. [23] combined the PV/T evaporator with the building roof to perform a theoretical study. The heat pump efficiency was over 70% along with the electrical and thermal efficiency of 55% and 19%. Bakker et al. [24] operated a 25 m^2 PV/T system and a ground heat pump; the electricity that the PV/T system generated could cover 96% electricity consumption of the system. Yang and Athienitis [25] summarized the different types of BIPV/T systems including the development and application of the various systems as well. Nižetić et al. [26, 27] used phase change material and pork fat as the coolant for PV applications, resulting in a reduction of the PV panel temperature to 10.26°C and an improvement in efficiency output of 3.73%.

In summary, the PV/T heat pump system can meet the diversified needs of building heating and domestic hot water at the same time. While the compressor and other components of the PV/T heat pump system consume a lot of electricity especially in hot summer, the refrigerant system can run in the form of a natural cycle or low power mechanical cycle to meet the demand. In contrast, the compressor in the PV/T heat pump system increases power consumption. Therefore, a PV/T façade system with a refrigerant pump was proposed [28] and experimental research was carried out. The PV/T module was applied as the evaporator, and the refrigerant (R134a) was used to produce the domestic hot water by absorbing heat energy through the PV modules. An air cavity between the PV/T modules and the external wall of the building was used for ventilation to avoid the extra cooling load due to the overheating of the external wall of the building. The experimental results show that, under the condition of the average solar radiation intensity of 496 W/m^2, the maximum heating COP of the system was 3.1, and the average electrical efficiency was 9% to meet the cogeneration. However, the research on the PV/T façade system is still under process, and there are various shortcomings in various aspects such as low solar cell convergence rate, the excessive temperature of the module, and the constant-frequency operation rate of the refrigerant pump.

There is some system deficiency laid out in Ref. [28] such as low solar cell coverage rate and poor heat transfer effect, the distribution of the refrigerant in the backchannel of the PV/T facade is heterogeneous, and the refrigerator pump can only run at the maximum speed of revolution. This paper, therefore, redesigned the device for the abovementioned problems: improved the PV/T module, redesigned the connection type, added the frequency variable pump, etc. The experiment will test the electrical efficiency, thermal efficiency, COP heating, and other output parameters of the PV/T façade system. For comparison, the photoelectric conversion characteristics of the PV/T façade system and the PV façade system were compared in an experiment. We evaluated and summarized the approaches used along with the enhanced performance of the proposed system.

2. Description of the PV/T Façade System

The hybrid PV/T façade module can transform solar energy into cogeneration production. The electric power is generated through photovoltaic modules, and the thermal energy is produced by extracting heat from the flat plate collector by the circulating refrigerant. The active opaque ventilated façade system proposed in Ref. [28] is a solar cogeneration system that integrates the hybrid PV/T module with the external façade of the building as shown in Figure 1. The size of a single component was 1.6 m × 0.9 m with the heat-collecting area of 1.44 m^2. The size of the solar cell was 156 mm × 156 mm, and the single module was made up of 36 cells which were connected in series having a packing factor of 60.8% as shown in Figure 1. Four PV/T module in the vertical direction were mounted and connected in series. The circulating form adopts the method of upside feed and underside flow. Therefore, the heat transfer of each piece of the PV/T module depends on the flow of the refrigerant. The connection form of the PV/T façade system is shown in Figure 1.

The refrigerant pump only operates at the maximum speed and cannot be adjusted according to the weather conditions. Under cloudy weather, the absorbed heat energy is insufficient due to the excessive flow, and a liquid hammer phenomenon could form, leading to the permanently impaired service life of the refrigerant pump, and reduces the efficiency of the system. The PV/T module faces the problem of low solar cell coverage rate and poor heat transfer effect. The inadequate contact area between the backchannel of the PV/T module and the plate collector leads to the incomplete evaporation of the refrigerant, so the thermal efficiency of the system was reduced. Moreover, it can be seen from Figure 2 that the temperature of the PV/T module at the bottom is significantly higher than that of the modules at high installation. This indicates that the refrigerant flow entering the PV/T module is not uniform and unable to absorb the heat of the PV/T module, resulting in the excessive temperature of the module at the bottom.

2.1. Improvement of the PV/T Façade System. To improve the performance of the PV/T façade system, this paper redesigned the connection form of the PV/T module for the building facade. The proposed roll-bond PV/T module is

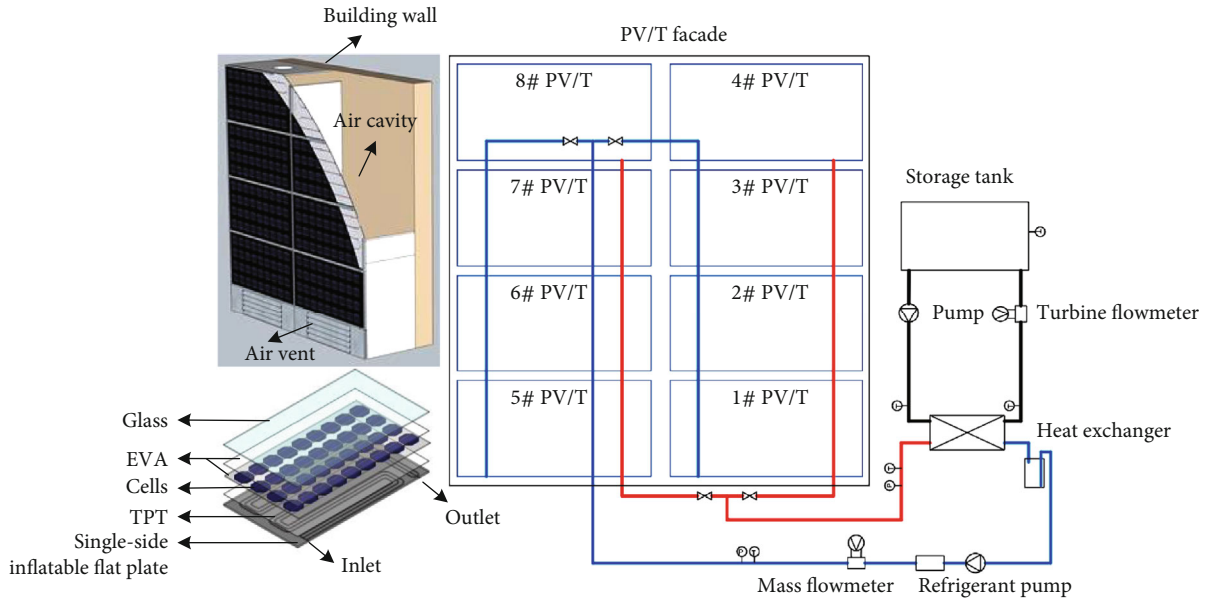

Figure 1: The connection form of the PV/T façade system before improvement [28].

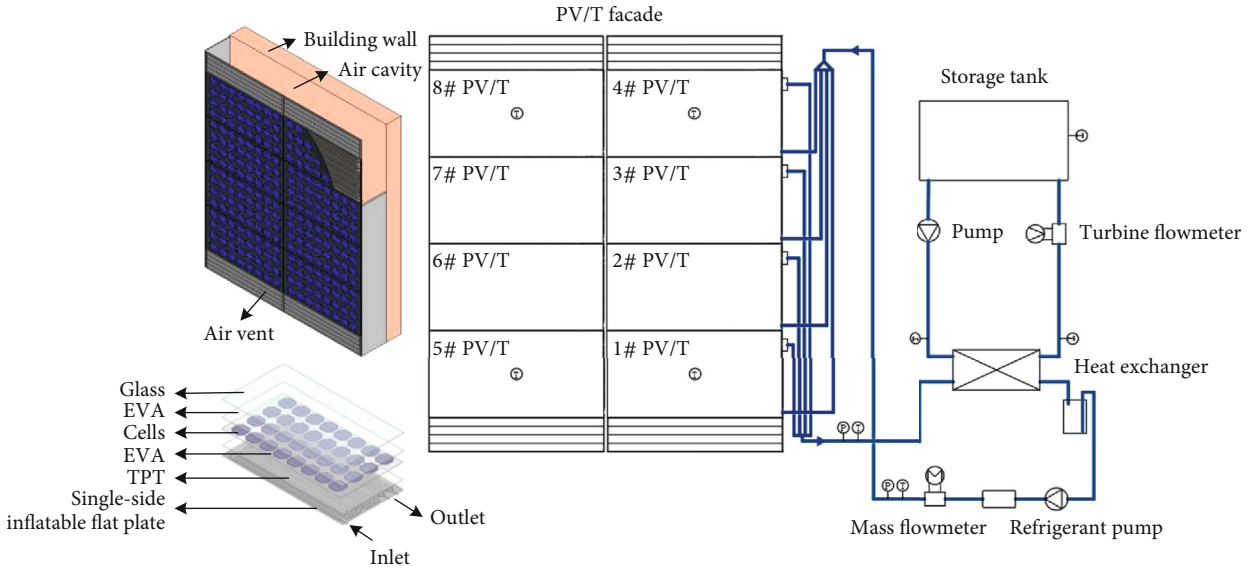

Figure 2: The infrared thermal imaging of the PV/T façade system.

composed of a glass cover plate, a photovoltaic cell sheet, TPT, an EVA adhesive, and a single-side inflatable flat plate collector [15]. The size of a single component is 1.56 m $\times$ 0.78 m with the heat-collecting area of 1.2 m^2. The size of the solar cell is 156 mm $\times$ 156 mm, and the single module is made up of 32 pieces which are connected in series having a packing factor of 64%. The back of the evaporating plate is a serpentine channel with a thickness of 2.5 mm. Under standard test conditions, the maximum heating power of the PV/T module is 800 W at the solar radiation intensity of 1000 W/m^2 and the ambient temperature is 25°C, and the maximum electrical efficiency is 16%. The proposed PV/T modules and their installations are shown in Figure 3.

To solve the problem of the nonuniform distribution of the refrigerant in the PV/T module of the vertical elevation, we have optimized the connection code and filling volume of the refrigerant of the PV/T module as follows:

(1) The connection form of the system is improved by using the liquid separator, as shown in Figure 3. At the inlet of the façade, a one-divided-into-four Venturi separator is used to separate the liquid, and the refrigerant is uniformly fed into each PV/T module. Besides, four modules are connected by the same program to ensure the resistance balance of each branch. Afterward, the refrigerant absorbs heat energy in the PV/T module and flows into the main pipeline

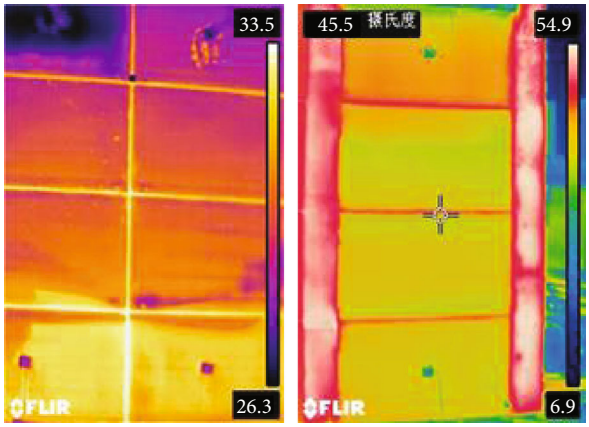

Before improvement After improvement

FIGURE 3: The connection form of the PV/T façade system after improvement.

(2) A liquid-phase volume method is adopted to calculate the amount of the refrigerant required by the system as given in Equation (1). The refrigerant is added into the system through a liquid adding valve on the main pipeline

$$M = 1.1\rho(V_P + 0.5V_E + 0.5V_C), \quad (1)$$

where M is the flow of the refrigerant (kg); 1.1 means a factor that accounts for the factors such as dissolving the refrigerant in the lubricating oil and neglecting the gas-phase medium; ρ is the saturated liquid density of the refrigerant under the average condensation temperature and evaporation temperature (kg/m^3); V_P is the volume of the liquid pipeline between the outlet of the tank and the inlet of the PV/T module (m^3); V_E is the volume of the refrigerant inside the PV/T module (m^3); and V_C is the volume of the refrigerant inside the heat exchanger (m^3).

According to the heat absorption capacity of the PV/T module under different working conditions, we have further considered the variable frequency pump. The flow range of the refrigerant of the PV/T module can be calculated. The speed of revolution of the refrigerant pump can be controlled by the frequency converter to change the mass flow to achieve the optimal operating state. Taking the thermodynamic performance of the PV/T module under the standard operating condition as an example, the maximum heating power is 800 W, assuming that the inlet working fluid of the PV/T module is saturated liquid and the temperature range is 20~40°C. The outlet working fluid is superheated steam, superheat is 5°C, and the temperature ranges from 25 to 45°C. According to Equation (2), the mass flow range of the refrigerant entering each PV/T module can be calculated which is 15.36~17.09 kg/h. The frequency converter is regulated to control the mass flow of the refrigerant entering each PV/T component based on the optimal mass flow range. The refrigerant flow matching weather conditions enables the system to operate under a stable and efficient state.

$$m_R = \frac{Q}{h_o - h_i}, \quad (2)$$

where m_R is the refrigerant flow rate (kg/h); Q is the maximum heating power of the PV/T module (W); h_i is the inlet refrigerant enthalpy (kJ/kg); and h_o is the outlet refrigerant enthalpy (kJ/kg).

2.2. Analysis of the Improved System. After the optimization and improvement in the PV/T façade system by methods described earlier, the infrared thermal imaging was used for comparison as shown in Figure 2. The temperature of the top PV/T module is between 33°C and 37°C. The temperature of the remaining PV/T modules under the first module is evenly distributed, with a temperature value of about 33°C. Since the vent is closed during the operation, the hot air in the cavity rises and accumulates at the place of the first PV/T module, and the temperature of the first PV/T module is higher than that of the following PV/T components.

Assume that the refrigerant in the first PV/T module absorbs heat and then completely evaporates and turns into superheated steam and the superheat is 4°C. The refrigerant in the following PV/T modules changes from liquid state to gas-liquid two-phase state after absorbing heat, and the temperature remains unchanged. By the first piece of inlet and outlet temperature of the PV/T module, according to Equation (2), the quantity of absorbed heat Q_1 of the first PV/T module can be calculated. The quantity of the obtained heat Q_s of water can be calculated by the inlet and outlet temperature of a heat exchanger. If Q_s is greater than Q_1, it states that the refrigerant inside the following PV/T modules has absorbed heat and turned into a gas-liquid phase. If Q_s is less than Q_1, it means that the following PV/T modules have not absorbed heat, and it is necessary to further check the system such as the dispenser and the pipeline. It is verified that the heat gain of water Q_s was greater than the heat absorption of the first PV/T module Q_1, so the refrigerant inside the following PV/T modules absorbed heat and changed from liquid phase to gas-liquid phase.

3. Experiment Layout

The PV/T façade system was installed on a westward vertical surface. In the afternoon, the external skin absorbed solar radiation, part of which was converted into electricity by solar cells, while most of them were converted into heat; the refrigerant in the rear of the PV/T modules absorbed heat energy, which was used to make domestic hot water.

The experimental system includes three parts: photoelectric, photothermal, and data acquisition systems. The photoelectric system mainly used the micro photovoltaic inverter by Envertech in measuring the output characteristic of solar cells; One inverter is connected to four pieces of PV/T modules, and another inverter is connected to four PV modules to conduct a comparative study. The two inverters are connected in series to the circuit breaker and then integrated into the grid, where the real-time generated power is recorded by

Table 1: Experimental devices used in the experiment.

Devices	Type	Range	Precision
Temperature sensor	Pt100	-20~100°C	±0.1°C
Pressure transmitter	CYYZ11-H	0~4 MPa	±0.25%FS
Wind speed transmitter	CHWVN	0~2 m/s	±0.2%FS
Turbine flowmeter	JST-LWG-10Y	0.15~1.5 m^3/h	±0.5%FS
Mass flowmeter	LHD8MH01	0~260 kg/h	±0.15/±0.20%
Three-phase wattmeter	FPW201	0~1 kW	±0.5%FS
Single-phase wattmeter	FPW101	0~1 kW	±0.5%FS
Pyranometer	TBQ-2		<5%FS
Inverter	EVT500		
Meteorological station	PC-4		
Modbus	RTU-318D		

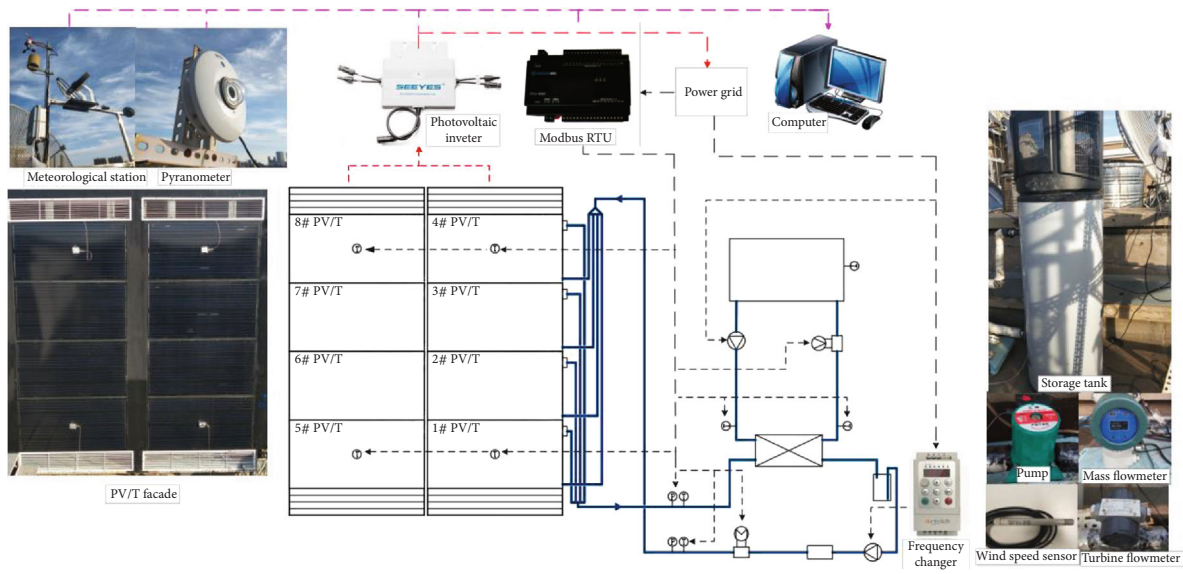

Figure 4: The proposed PV/T façade system.

the monitor and uploaded to a database for storage. The photothermal system is mainly composed of a PV/T module, refrigerant pump, plate heat exchanger, water pump, and storage tank. After absorbing heat through the PV/T modules, the refrigerant enters the plate heat exchanger to exchange heat with water. Afterward, it was again pumped into the PV/T façade by the refrigerant pump to complete a cycle. The data acquisition system mainly includes the measurement of temperature, pressure, flow rate, wind speed, irradiance, and other parameters. The necessary instruments are shown in Table 1. Modbus RTU combined with wireless communication is applied in real-time acquiring and monitoring data displayed as data tables or curve graphs on the web and app. Parameters such as irradiance and wind speed can be measured by meteorological stations.

The experimental process was tested following the test method for the thermal performance of flat plate solar collectors [29]. Temperature sensors were arranged on PV/T and PV modules at the front and rear. Three temperature sensors are uniformly arranged on the solid wall, and their average value is taken as the temperature of the solid wall. Five temperature sensors are arranged in the air chamber between the façade skin and the solid wall, and the average value is taken as the temperature of the air chamber. Temperature sensors are also placed in the middle of the tank and the inlet and outlet of the exchanger. Moreover, sensors are placed at the inlet and outlet of the PV/T façade to measure the temperature and pressure of the refrigerant. The mass flowmeter and turbine flowmeter are used to measure the flow of refrigerant and water, respectively. During the experiment, the data for each parameter were recorded every five minutes. The description of the experimental facility is shown in Figure 4.

3.1. Performance Evaluation. The heating capacity of the PV/T façade system can be calculated by the following formula:

$$Q_w = \rho C_p V \left[T_{w,\tau_2} - T_{w,\tau_1}\right], \tag{3}$$

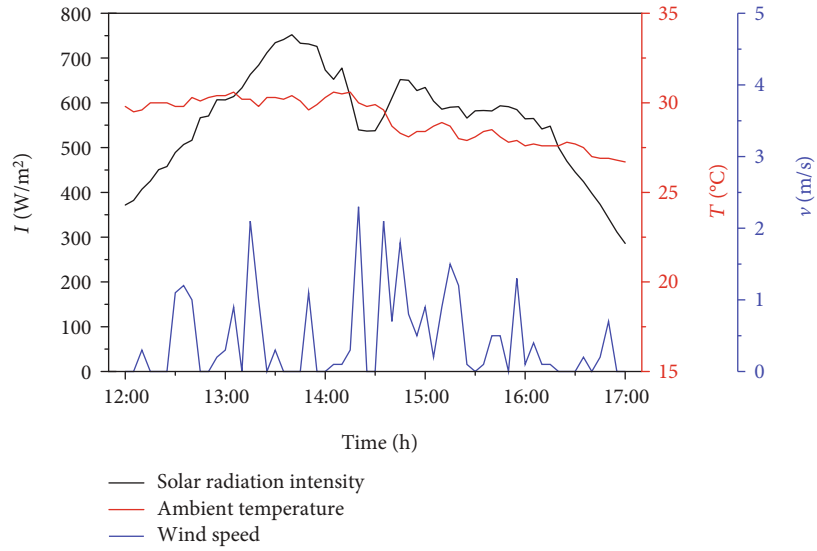

Figure 5: The curve of solar radiation intensity and ambient temperature.

where Q_w is heating capacity (kJ); ρ is the density of water (kg/m^3); C_p is the specific heat of water (kJ/(kg·°C)); V is volume (m^3); ($T_{w,\tau 1}$) is the initial temperature of the water in the tank (°C); and $T_{w,\tau 2}$ is the final temperature of the water in the tank (°C).

The heating COP of the PV/T façade system can be calculated by the following formula:

$$\mathrm{COP} = \frac{Q_w}{\sum(W_R + W_W)}, \tag{4}$$

where COP is thermal performance coefficient of the system; W_R is refrigerant pump power consumption (W); and W_w is water pump power consumption (W.)

The thermal efficiency of the PV/T façade system is

$$\eta_{th} = \frac{Q_w}{IA_{PV/T}}, \tag{5}$$

where η_{th} is thermal efficiency (%); I is the amount of solar radiation (W/m^2); and $A_{PV/T}$ is the PV/T module area (m^2).

The electrical efficiency formula is as follows:

$$\eta_e = \frac{P}{IA_{PV}}, \tag{6}$$

where η_e is electrical efficiency (%); P is the power generated by photovoltaic cells (W); and A_{PV} is the PV area (m^2).

Because of the difference in energy grade between electrical energy and thermal energy, a direct comparison of their combined efficiency with the conversion efficiency of other photoelectric or photothermal devices is not appropriate. The conversion of photoelectric power to heat energy is therefore considered, which is convenient for comparison with the conversion efficiency of ordinary photoelectric-thermal or photoelectric conversion devices. The comprehensive performance of the PV/T façade system is

$$\eta_s = \frac{\eta_e}{\eta_{power}} + \eta_{th}, \tag{7}$$

where η_s is the comprehensive performance of the PV/T façade system (%) and η_{power} is the generation efficiency of conventional thermal power, the value of 0.38 [3].

4. Results and Discussion

To evaluate the performance of the improved PV/T façade system, experiments were conducted from September to October 2019. We have taken September 29 experimental data for analysis. The air vent was closed during the experiment. The experiment was conducted from 12:00 to 17:00, and the recording interval of each parameter was 5 minutes. Figure 5 shows the curve of solar radiation intensity and ambient temperature during the testing period. It can be seen that the highest temperature during the test period was 30.6°C, and the average temperature was 29.0°C. The maximum wind speed was 2.3 m/s, and the average wind speed was 0.4 m/s. The maximum radiation intensity of the west facade is 752.15 W/m^2, and the average radiation intensity is 562 W/m^2. The volume of the storage tank is 150 L, and the initial tap water temperature is 23°C.

The heating COP, the thermal efficiency, and the temperature of the tank with time are shown in Figure 6. During the test period, the temperature of the tank continues to rise from 23°C to 39.4°C, with a total heat of 10.33 MJ. The heating COP and thermal efficiency of the PV/T façade system show a similar downward trend. The temperature of the tank decreases with the dropping of heating COP. The average COP of the system was 3.4, and the average thermal efficiency

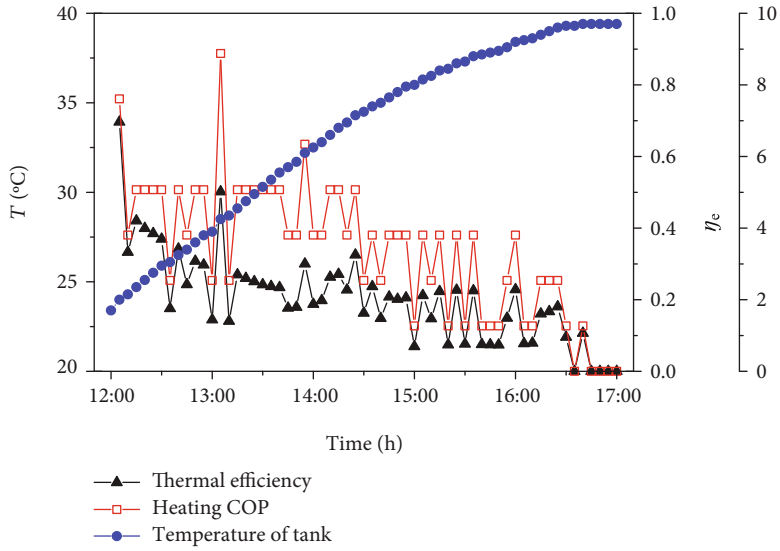

Figure 6: Curves of the heating COP, the temperature of the tank, and thermal efficiency.

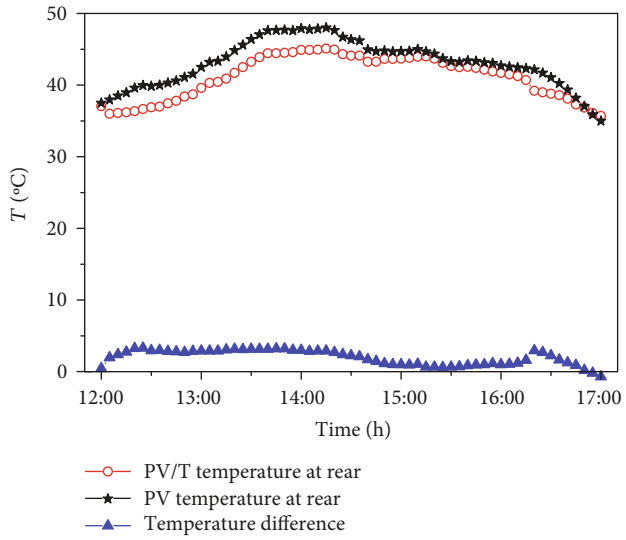

Figure 7: Temperature variation of different façade.

was 20% throughout the experiment. The thermal efficiency of the PV/T system is considerable, and the hot water can be used for domestic purposes.

Figure 7 shows the temperature of the PV/T and PV façade over time. As can be seen from the figure, the temperature of PV/T at rear increases from 37°C to 45°C, with a temperature change of 8°C. The temperature of PV at rear increases from 37°C to 48°C, and the temperature changes by 11°C. The temperature fluctuation of PV/T at the rear is relatively small, which can avoid the drastic fluctuations of façade temperature caused by the sudden changes in solar radiation intensity during the operation. Thus, the PV/T system could maintain a more stable operating state.

Figure 8 shows the comparison of the electrical efficiency of the PV/T and PV façade system. During the test period, the average solar radiation intensity was 562 W/m^2, the average temperature was 29°C, the PV/T façade system generated 0.72 kW·h, and the average electrical efficiency was 8%, whereas the total power generation of the PV façade system is 0.63 kW·h, with an average electrical efficiency of 7%. The electrical efficiency of the PV/T façade system is 14.3% which is higher than that of the PV façade system. The power generation of the PV/T façade system was 0.95 kW·h throughout the day. Meanwhile, the power consumption was 0.83 kW·h. When the solar radiation intensity reached the maximum, the electrical efficiency of the PV/T and PV façade system did not reach the peak. The reason is that the ambient temperature is relatively high, which leads to the temperature rise of cells; thus, the electrical efficiency decreases. Before 15:00, with the decrease of ambient temperature and the solar radiation intensity also maintained at a high range, the electrical efficiency gradually increases.

Figure 9 shows the curve of the comprehensive efficiency of the PV/T façade system over time. Throughout the test, the average comprehensive efficiency is 42%, and the comprehensive efficiency decreased from the maximum value of 60% to a minimum of 10%. During the period of 12:00~14:00, the comprehensive efficiency decreased slowly; after 16:00, due to the sudden drop in solar radiation intensity, the comprehensive efficiency of the system changed sharply. The improved PV/T system has excellent comprehensive efficiency and wide application prospect.

Since the meteorological conditions of the current study are different from those listed in Ref. [28], the meteorological conditions include solar radiation intensity, ambient temperature, and wind speed. To reasonably compare the heating COP, the Gaussian mixture model (GMM) was adopted to cluster the meteorological data. The classification and clustering problems are different. In the classification problem, the classification property value of the sample is acquainted, whereas in the clustering problem, the classification property value needs to be found. Therefore, the classification problem is called unsupervised learning, and the clustering problem is

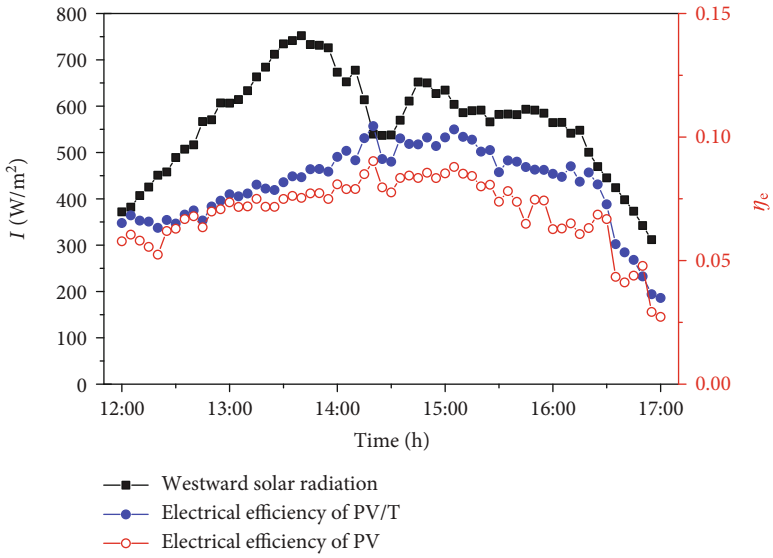

Figure 8: The electrical efficiency of the PV/T and PV façade system.

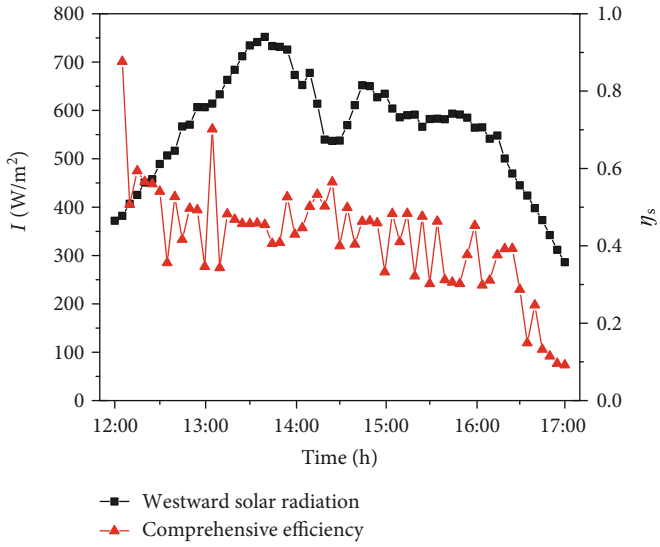

Figure 9: The comprehensive efficiency of the PV/T façade system.

called supervised learning. Assuming that the data obey the Gaussian distribution, different clusters correspond to different Gaussian distribution parameters, which is the principle of the GMM. After processing the data, the required clustering results will be obtained by using probability as the measurement standard. The meteorological data in this paper are taken as reference points, and the data in reference [28] are clustered to obtain conditions similar to the meteorological data presented in this paper.

The definition formula of the GMM is as follows:

$$P(x) = \sum_{k=1}^{k} \pi_k P\left(x \mid \mu_k, \sum_k\right), \tag{8}$$

where π_k is a weight for each cluster distribution, which means the probability of category k; μ_k is the mean vector of the cluster distribution; $\sum_k$ is the covariance matrix of the cluster distribution; and $P(x \mid \mu_k, \sum_k)$ is the posterior probability of sample x generated by the kth cluster distribution.

The key to solving the GMM problem is calculated from the parameters of π_k, $\sum_k$, and $P(x \mid \mu_k, \sum_k)$, so the EM algorithm is adopted. Briefly, the EM algorithm uses two steps to compute alternately. The first step is the E step (expectation step), which uses the currently estimated parameter to calculate the expectation of log-likelihood estimation, and the second step is the M step (maximization step), finding the parameter which maximizes the expectation of the log-likelihood calculated by the E step. Then, the newly obtained parameter is reused for the E step, until it converged to the local optimal solution.

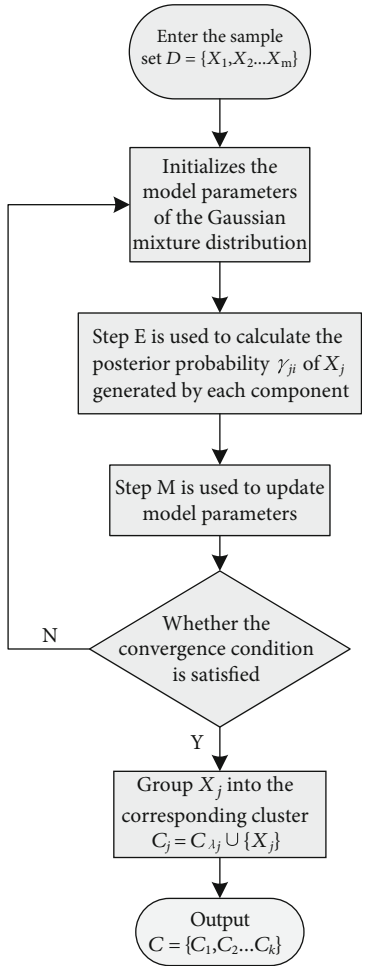

Figure 10: The workflow of GMM.

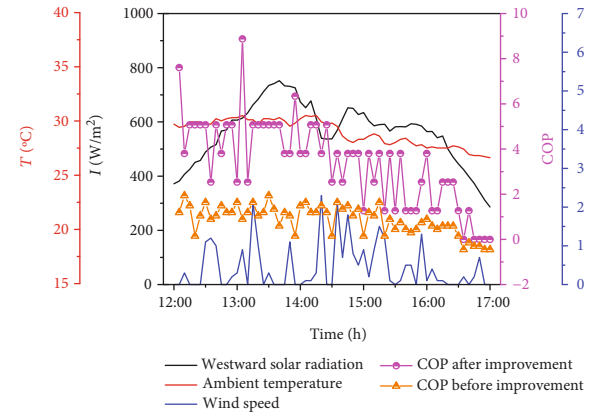

Figure 11: The comparison curves of heating COP under similar conditions.

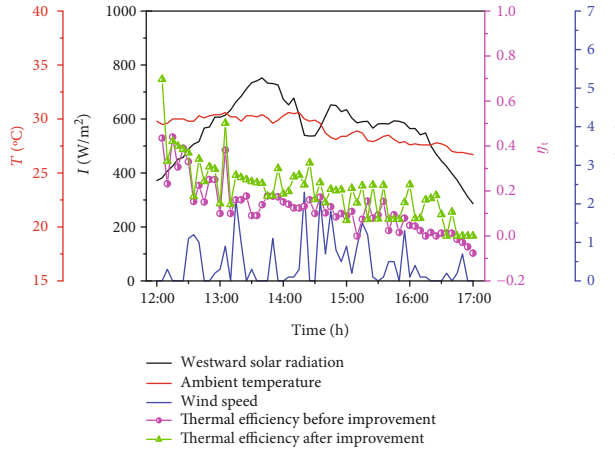

Figure 12: The comparison curves of thermal efficiency under similar conditions.

Figure 10 shows the workflow diagram of the GMM. The sample-set $D = \{x_1, x_2 \cdots x_m\}$ contains m samples, and each sample $x_1 = (I_1, t_1, v_1)$ is a three-dimensional feature vector. Through GMM, the sample set D is divided into k disjoint clusters $\{C_l \mid l = 1, 2, \cdots, k\}$; accordingly, $\lambda_j \in \{1, 2, \cdots, k\}$ represents the cluster tag of sample x_j, that is, $x_j \in C_{\lambda j}$; thus, the results $C = \{C_1, C_2, \cdots, C_k\}$ is obtained; then, the heating COP can be compared under similar working conditions.

Figure 11 represents the comparison curves of heating COP under similar conditions. It can be seen from the figure that the heating COP before and after improvement shows a similar downward trend. However, with a similar operation, the average COP of this work is about 3.4 which is higher than 0.9 [28]. The heating COP of the PV/T façade system is significantly promoted after improvement in the PV/T façade system. The improved system has more energy-saving advantages.

Figure 12 shows the comparison curves of thermal efficiency under similar conditions; it is evident that the trend of the thermal efficiency of the PV/T façade system after improvement is decreasing gradually the same as that of the PV/T façade system before improvement, whereas the thermal efficiency of the PV/T façade system after improvement is much higher. The average thermal efficiency of the PV/T façade system is 20% which is higher than 13% of the system before improvement. Through the improvements described above, the performance of the PV/T façade system raised significantly.

5. Conclusions

This study presented the BIPV/T façade system driven by a refrigerant pump. The BIPV/T façade system was improved by redesigning the traditional system of BIPV/T. The heating COP, thermal efficiency, electrical efficiency, and the comprehensive performance of the BIPV/T façade system were evaluated through experimental tests. A comparison of the proposed BIPV/T system with the traditional system has been made. The following conclusions were drawn, based on the results of the experimental test:

(1) The total heat output of the BIPV/T façade system was 10.33 MJ during 12:00~17:00, the system 's average heating COP was 3.4, and the average thermal efficiency was 20%

(2) The BIPV/T façade system modules can sustain a lower temperature as opposed to the PV façade system, thereby improving the electrical performance. The PV/T system's electrical efficiency was 14.3% higher throughout the test than that of the PV façade system

(3) The thermal efficiency of the PV/T façade system was 20% during the experimental period, the electrical efficiency was 8%, and the overall efficiency was 42%

(4) This study's average heating COP was 3.4, above the presented 0.9 in the Ref. [28]

(5) The average PV/T façade system thermal efficiency reached 20%, higher than the conventional system with 13%

Nomenclature

A_{PV}: PV module area
$A_{PV/T}$: PV/T module area
C_p: Specific heat of the water
h_i: The inlet refrigerant enthalpy
h_o: The outlet refrigerant enthalpy
I: The amount of solar radiation in the west elevation
M: The flow of the refrigerant
m_R: The refrigerant flow rate
P: The power generated by photovoltaic cells
Q: The maximum heating power of PV/T module
Q_s: The quantity of obtained heat of the water
Q_1: The quantity of absorbed heat of the first PV/T module
Q_w: Heating capacity
$T_{w,\tau 1}$: The initial temperature of the water in the tank
$T_{w,\tau 2}$: The final temperature of the water in the tank
V_P: The volume of the liquid pipeline between the outlet of the tank and the inlet of the PV/T module
V_E: The volume of the refrigerant inside the PV/T module
V_C: The volume of the refrigerant inside the heat exchanger
V: Volume
W_R: Refrigerant pump power consumption
W_w: Water pump power consumption.

Greek Symbols

ρ: The liquid density
η_e: Electrical efficiency
η_{power}: The generation efficiency of conventional thermal power
η_s: The comprehensive performance of the PV/T façade system
η_{th}: Thermal efficiency.

Abbreviations

APP: Application
BIPV: Building-integrated photovoltaic
BIPV/T: Building-integrated photovoltaic/thermal
COP: Thermal performance coefficient of the system
PV: Photovoltaic
PV/T: Photovoltaic/thermal.

Data Availability

The raw/processed data required to reproduce these findings cannot be shared at this time as the data also form part of an ongoing study.

Additional Points

Highlights. (1) The solar cogeneration façade system driven by a refrigerant pump was designed. (2) An experimental system of the active opaque ventilated façade was established. (3) Improved performance of the system was carried out with outdoor climatic conditions

Conflicts of Interest

The authors declare no conflict of interest.

Acknowledgments

This research is supported by the National Key Research and Development Project of China No. 2017YFC0704100 (entitled New generation intelligent building platform techniques), the National Natural Science Foundation of China (No.51806029) and (No.61803067), and the Fundamental Research Funds for the Central Universities of China (DUT20JC15).

References

[1] Chinese academy of engineering, *Key Technologies and Development Prospects of Global Energy Internet Connection*, Higher Education Press, Beijing, 2018.

[2] C. Guo, *Numerical and experimental study of tri-functional photovoltaic/thermal collector [D]*, University of Science and Technology of China, Hefei, 2015.

[3] G. Pei, "Study on photovoltaic-solar assisted heat pump system and multifunctional domestic heat pump system [D].," University of Science and Technology of China, Hefei, 2006.

[4] T. Kim, B.-I. Choi, Y.-S. Han, and K. H. Do, "A comparative investigation of solar-assisted heat pumps with solar thermal collectors for a hot water supply system," *Energy Conversion and Management*, vol. 172, pp. 472–484, 2018.

[5] M. T. Plytaria, C. Tzivanidis, E. Bellos, and K. A. Antonopoulos, "Energetic investigation of solar assisted heat pump underfloor heating systems with and without phase change materials," *Energy Conversion and Management*, vol. 173, pp. 626–639, 2018.

[6] S. Vaishak and P. V. Bhale, "Photovoltaic/thermal-solar assisted heat pump system: current status and future prospects," *Solar Energy*, vol. 189, pp. 268–284, 2019.

[7] E. Zanetti, M. Aprile, D. Kum, R. Scoccia, and M. Motta, "Energy saving potentials of a photovoltaic assisted heat pump for hybrid building heating system via optimal control," *Journal of Building Engineering*, vol. 27, p. 100854, 2020.

[8] A. Riaz, R. Liang, C. Zhou, and J. Zhang, "A review on the application of photovoltaic thermal systems for building façades," *Building Services Engineering Research & Technology*, vol. 41, no. 1, pp. 86–107, 2020.

[9] M. Li, T. Ma, J. Liu et al., "Numerical and experimental investigation of precast concrete facade integrated with solar photovoltaic panels," *Applied Energy*, vol. 253, p. 113509, 2019.

[10] A. C. F. Maciel and M. T. Carvalho, "Operational energy of opaque ventilated façades in Brazil," *Journal of Building Engineering*, vol. 25, p. 100775, 2019.

[11] D. Zhang, Q. B. Wu, J. P. Li, and X. Q. Kong, "Effects of refrigerant charge and structural parameters on the performance of a direct-expansion solar-assisted heat pump system," *Applied Thermal Engineering*, vol. 73, no. 1, pp. 522–528, 2014.

[12] C. Lertsatitthanakorn, J. Jamradloedluk, M. Rungsiyopas, A. Therdyothin, and S. Soponronnarit, "Performance analysis of a thermoelectric solar collector integrated with a heat pump," *Journal of Electronic Materials*, vol. 42, no. 7, pp. 2320–2325, 2013.

[13] A. A. Ammar, K. Sopian, M. A. Alghoul, B. Elhub, and A. M. Elbreki, "Performance study on photovoltaic/thermal solar-assisted heat pump system," *Journal of Thermal Analysis and Calorimetry*, vol. 136, no. 1, pp. 79–87, 2019.

[14] X. Sun, J. Wu, Y. Dai, and R. Wang, "Experimental study on roll-bond collector/evaporator with optimized-channel used in direct expansion solar assisted heat pump water heating system," *Applied Thermal Engineering*, vol. 66, no. 1-2, pp. 571–579, 2014.

[15] C. Zhou, R. Liang, A. Riaz, J. Zhang, and J. Chen, "Experimental investigation on the tri-generation performance of roll-bond photovoltaic thermal heat pump system during summer," *Energy Conversion and Management*, vol. 184, pp. 91–106, 2019.

[16] J. Jie, H. Wei, and H. Lam, "The annual analysis of the power output and heat gain of a PV-wall with different integration mode in Hong Kong," *Solar Energy Materials and Solar Cells*, vol. 71, no. 4, pp. 435–448, 2002.

[17] R. A. Agathokleous, S. A. Kalogirou, and S. Karellas, "Exergy analysis of a naturally ventilated building integrated photovoltaic/thermal (BIPV/T) system," *Renewable Energy*, vol. 128, no. PB, pp. 541–552, 2018.

[18] R. A. Agathokleous and S. A. Kalogirou, "Part I: thermal analysis of naturally ventilated BIPV system: experimental investigation and convective heat transfer coefficients estimation," *Solar Energy*, vol. 169, pp. 673–681, 2018.

[19] R. A. Agathokleous and S. A. Kalogirou, "Part II: thermal analysis of naturally ventilated BIPV system: modeling and simulation," *Solar Energy*, vol. 169, pp. 682–691, 2018.

[20] L. Keliang, J. Jie, C. Tin-tai et al., "Performance study of a photovoltaic solar assisted heat pump with variable- frequency compressor – A case study in Tibet," *Renewable Energy*, vol. 34, no. 12, pp. 2680–2687, 2009.

[21] J. Ji, G. Pei, T.-t. Chow et al., "Experimental study of photovoltaic solar assisted heat pump system," *Solar Energy*, vol. 82, no. 1, pp. 43–52, 2008.

[22] J. Ji, H. He, T. Chow, G. Pei, W. He, and K. Liu, "Distributed dynamic modeling and experimental study of PV evaporator in a PV/T solar-assisted heat pump," *International Journal of Heat and Mass Transfer*, vol. 52, no. 5-6, pp. 1365–1373, 2009.

[23] X. Zhao, X. Zhang, S. B. Riffat, and Y. Su, "Theoretical study of the performance of a novel PV/e roof module for heat pump operation," *Energy Conversion and Management*, vol. 52, no. 1, pp. 603–614, 2011.

[24] M. Bakker, H. A. Zondag, M. J. Elswijk, K. J. Strootman, and M. J. M. Jong, "Performance and costs of a roof-sized PV/thermal array combined with a ground coupled heat pump," *Solar Energy*, vol. 78, no. 2, pp. 331–339, 2005.

[25] T. Yang and A. K. Athienitis, "A review of research and developments of building-integrated photovoltaic/thermal (BIPV/T) systems," *Renewable and Sustainable Energy Reviews*, vol. 66, pp. 886–912, 2016.

[26] S. Nižetić, M. Arıcı, F. Bilgin, and F. Grubišić-Čabo, "Investigation of pork fat as potential novel phase change material for passive cooling applications in photovoltaics," *Journal of Cleaner Production*, vol. 170, pp. 1006–1016, 2018.

[27] M. Arıcı, F. Bilgin, S. Nižetić, and A. M. Papadopoulos, "Phase change material based cooling of photovoltaic panel: a simplified numerical model for the optimization of the phase change material layer and general economic evaluation," *Journal of Cleaner Production*, vol. 189, pp. 738–745, 2018.

[28] R. Liang, Q. Pan, P. Wang, and J. Zhang, "Experiment research of solar PV/T cogeneration system on the building façade driven by a refrigerant pump," *Energy*, vol. 161, pp. 744–752, 2018.

[29] GB/T 4271—2000, *Test methods for the thermal performance of flat plate solar collectors*, Standards Press of China, Beijing, 2000.